Nature Communications

https://doi.org/10.1038/s41467-026-70380-9

Article in Press

A bionic robotic trunk with tensegrity-enabled elephant-comparable stiffness variability for assisted daily living

Received: 4 July 2025

Accepted: 16 February 2026

Cite this article as: Zhang, J., Yang, C., Yang, H. *et al.* A bionic robotic trunk with tensegrity-enabled elephant-comparable stiffness variability for assisted daily living. *Nat Commun* (2026). https://doi.org/10.1038/s41467-026-70380-9

Jie Zhang, Chaozhong Yang, Hao Yang, Pengfei Ma, Chenyu He, Teng Zhang, Xiaofeng Wang, Ke Liu, Xiu Jia & Haijun Peng

A bionic robotic trunk with tensegrity-enabled elephant-comparable stiffness variability for assisted daily living

Jie Zhang[1, 2, #], Chaozhong Yang[1, #], Hao Yang[1], Pengfei Ma[1], Chenyu He[1], Teng Zhang[3], Xiaofeng Wang[4], Ke Liu[5], Xiu Jia[6, *], Haijun Peng[1, 2, *]

[1]School of Mechanics and Aerospace Engineering, Dalian University of Technology, Dalian, China

[2]State Key Laboratory of Structural Analysis, Optimization and CAE Software for Industrial Equipment, Dalian University of Technology, Dalian, China

[3]Department of Mechanical and Aerospace Engineering, Syracuse University, Syracuse, New York, USA

[4]Central Hospital, Dalian University of Technology, Dalian, China

[5]School of Advanced Manufacturing and Robotics, Peking University, Beijing, China

[6]Department of Modern Mechanics and Institute of Humanoid Robots, University of Science and Technology of China, Hefei, China

[#]These authors contributed equally to this study.

*Corresponding authors: jiaxiu05@ustc.edu.cn (X. J); hjpeng@dlut.edu.cn (H. P)

Abstract:

Elephant trunks can rapidly vary their stiffness over a broad range, seamlessly switching between soft states for dexterous operation and rigid states for load-bearing tasks. Despite extensive efforts to mimic this stiffness variability using various approaches, such as jamming structures and phase-change materials, existing bionic robots are limited to narrow tunable stiffness ranges and/or slow switching frequencies. In this work, we present a bionic robotic trunk with a cable-driven tensegrity skeleton, leveraging synergistic and antagonistic muscle-mimicking mechanisms to achieve dynamic stiffness regulation. Through coordinated contraction of motor-actuated cables (i.e., antagonistic action), the robotic trunk achieves a stiffness range of 23.94 to 542.47 N/m and a switching frequency of 1.06 Hz, matching the adaptability of elephant trunks. This rapid and large-scale stiffness variation enables dexterous navigation in unstructured environments and powerful manipulation of heavy objects. Incorporated into an electric wheelchair with the human-machine interface, the robotic trunk assists a post-stroke individual with daily activities, such as opening cabinet doors, retrieving milk from refrigerators, and watering flowers. This work advances bio-inspired robotics and highlights the potential of stiffness-tunable robotic trunks in assistive applications.

Keywords: bionic robotic trunk, tensegrity skeleton, stiffness modulation, switching frequency, mobile robotic system

1. Introduction

Elephant trunks, with their nearly infinite number of degrees of freedom (DoFs), exemplify an extraordinary balance of dexterity and strength[1]. Their soft and compliant nature enables delicate tasks such as peeling a banana, while still allowing them to lift loads up to 270 kg[2,3]. Despite their complex muscular structure, elephant trunks perform rapid, precise movements across diverse tasks, largely thanks to their ability to rapidly modulate stiffness through synergistic and antagonistic muscle actions[3,4].

Inspired by this biological marvel, decades of research have focused on developing soft robots mimicking elephant trunks[5-9]. Currently, three primary approaches are commonly used to realize unique stiffness variability: mechanical locking structures[10-12], pneumatic jamming systems[13-15], and phase-change materials[16-18]. Mechanical locking structures utilize body friction or geometric constraint to lock specific configurations, adjusting stiffness for diverse tasks[19,20]. Pneumatic jamming systems modulate the stiffness by varying the pressure to alter friction between particles, fibers, or layers within fluidic channels[21-23]. Phase-change materials, such as shape memory alloys (SMAs) and low melting point alloys (LMPAs), exploit temperature-induced phase transition to reversibly change material stiffness[24,25]. However, each approach has notable limitations[26]. For example, mechanical locking structures provide only discrete stiffness states, lacking continuous modulation observed in elephant trunks[27]. Pneumatic jamming systems usually involve bulky external pumps or vacuum sources to adjust the pressure[28,29]. Phase-change materials, while capable of continuous stiffness changes, suffer from their prolonged actuation cycles, e.g., the notoriously slow cooling process of SMAs[30,31].

An alternative strategy, directly inspired by the elephant's biology, leverages synergistic and antagonistic mechanisms to modulate stiffness[32-36]. Synergistic mechanisms involve the

coordinated contraction/extension of multiple actuators working together to reduce overall stiffness, allowing for soft and compliant motion[37]. Conversely, antagonistic mechanisms rely on opposing actuator actions that generate counterbalancing forces, rapidly increasing stiffness for loading-bearing tasks[27]. Although this approach provides a simple and effective means of stiffness modulation without additional complex structures or materials, existing implementations-particularly in cable-driven systems-fail to match the stiffness modulation performance of biological trunks. The primary limitation of existing designs is that their antagonistic actions depend solely on the elastic deformation of actuators-such as cables-while the main structure remains nearly undeformed, resulting in only slight variations in elastic energy and thus a limited stiffness range. For instance, soft continuum robots proposed by Kim et al. exhibited tunable stiffness through synergistic and antagonistic actions of the cables, enhancing adaptive capability for robotic single-port surgery[38]. However, buckling in the main structure introduces structural instability during antagonistic actions. This instability restricts the large-scale increase in elastic energy, thereby resulting in stiffness that can only be tuned within a narrow range[39,40].

In this study, we present a bionic robotic trunk (BRT) that leverages synergistic and antagonistic mechanisms to implement rapid and wide-range stiffness modulation (Fig. 1A). Inspired by the biomechanics of elephant trunks, which modulate internal stiffness through active tensioning of antagonistic muscles to redistribute elastic energy [3], our BRT adopts a cable-driven tensegrity skeleton—a lightweight and compliant architecture that can redistribute elastic energy via cable-induced deformation of struts and springs[41,42]. Within this skeleton, synergistic actuator contractions enable soft and compliant movements, while antagonistic actions increase stiffness significantly, as showcased in Fig. 1B. Enabled by reconfigurable tensegrity, stored elastic energy is increased by 10 times at antagonistic configuration, yielding stiffness ranging from 23.94 to

542.47 N/m at switching frequency of 1.06 Hz, comparable to that of the elephant trunk (Fig. 1C, Table S1)[20,28,37,39,43-53]. Subsequently, positional finite element analysis further elucidates the underlying stiffness modulation mechanism. The BRT's rapid response and broad stiffness range enable it to dynamically adapt to diverse demands and external stimuli. To demonstrate its practical utility, we integrate the BRT into an electric wheelchair with a human-machine interface, showcasing its effectiveness in assisting individuals with daily activities, such as opening cabinet doors, retrieving items from refrigerators, and watering flowers (Fig. 1D). By combing flexibility, strength, and efficiency, the BRT establishes a new benchmark for robotic trunk design, providing a versatile solution for navigating complex environments and assistive robotics.

2. Results

2.1 Tensegrity-based Design of BRT

We proposed a tensegrity-based BRT (length: 920 mm and weight: 1.05 kg) that achieves both dexterous morphing and powerful load-bearing capabilities through controlled cable interactions. As shown in Fig. 2A, the BRT consists of three main sections: the basal, middle, and distal portions. The basal portion is a rigid disk with six prefabricated holes, through which six actuation cables (No. 1-6) are threaded. Notably, to avoid potential stress hysteresis issues during cable stretching, we pre-stretched these cables 500 times before integrating them into the robotic system (Supplementary Fig. 1). The middle and distal portions each contain nine identical rigid frames (denoted as $\mathcal{F}_i,\ i = 1, \ldots, 9$), which are actuated by cables No. 1-3 and cables No. 4-6, respectively. Additionally, to prevent physical interference between these two sets of cables, cables No. 4-6 are enclosed in stiff sheaths, and pass through the pre-fabricated hole in the distal portion, bypassing the middle portion (Supplementary Fig. 2 and Movie 1).

Each rigid frame in the middle and distal portions consists of three struts denoted as $\mathcal{F}_i^1\mathcal{F}_i^2$,

$\mathcal{F}_i^3\mathcal{F}_i^4$, and $\mathcal{F}_i^5\mathcal{F}_i^6$ that converge at the central node $\mathcal{F}_i^0$, where the superscript 0-6 denotes nodes on the frame. Two types of springs-connecting springs and reinforcing springs-are used to link frames $\mathcal{F}_i$ and $\mathcal{F}_{i+1}$. Three connecting springs (labeled as $\mathcal{S}_{cj},\ j = 2,4,6$) ensure structural continuity and flexible assembly by linking the central node $\mathcal{F}_i^0$ on the frame $\mathcal{F}_i$ to the nodes $\mathcal{F}_{i+1}^2$, $\mathcal{F}_{i+1}^4$, and $\mathcal{F}_{i+1}^6$ on frame $\mathcal{F}_{i+1}$. Another three connecting springs ($\mathcal{S}_{cj},\ j = 1,3,5$) attach the central node $\mathcal{F}_{i+1}^0$ to the nodes $\mathcal{F}_i^1$, $\mathcal{F}_i^3$, and $\mathcal{F}_i^5$ of the frame $\mathcal{F}_i$, reinforcing the alignment and stability. To further enhance structural integrity, two reinforcing springs ($\mathcal{S}_{\mathrm{r}j},\ j = 1,2$) connect node $\mathcal{F}_i^5$ of frame $\mathcal{F}_i$ to nodes $\mathcal{F}_{i+1}^2$ and $\mathcal{F}_{i+1}^4$ of the frame $\mathcal{F}_{i+1}$. The effectiveness of these reinforcing springs is showcased in Fig. 2B, which compares the centerline alignment of the BRT with and without reinforcing springs. The Z-coordinate of the centerline quantifies structural sagging due to gravity: in the reinforced BRT, the last frame maintains a Z-coordinate of -0.15 cm, whereas in the non-reinforced BRT, the last frame sags significantly to -6.63 cm. This result confirms that reinforcing springs help maintain a centralized alignment against gravitational forces, thereby reducing unwanted deformation. The arrangement of reinforcing springs is also equally effective in minimizing the influence of gravity when placed in vertical directions (Supplementary Fig. 3).

In addition to minimizing structural sagging, reinforcing springs also improve twisting stiffness, enhancing torsional resistance during movement. As shown in Supplementary Fig. 4, the twisting angle is measured for both configurations, revealing that the non-reinforced structure exhibits nearly twice the twisting deformation compared to the reinforced version. Fig. 2C further quantifies twisting stiffness, showing that the reinforced BRT has significantly greater resistance to torsional forces.

2.2 Tensegrity-enabled large-scale stiffness modulation of BRT

The core functionality of the BRT is to continuously and rapidly modulate stiffness over a broad range, enabling transitions between soft, compliant deformation and rapid, load-bearing behavior. This functionality is intrinsically enabled by the tensegrity structure and the controlled coordination of cable actuation, inspired by synergistic and antagonistic muscular mechanisms.

As shown in Fig. 3A, a low-stiffness state is achieved through synergistic actuation, in which cables 2, 3, 5, and 6 are pulled while cables 1 and 4 are released. This asymmetric configuration induces simultaneous downward and upward bending in the middle and distal portions, forming an S-shaped morphology. This allows the BRT to perform diverse bending configurations (Supplementary Fig. 5) that gives rise to a large workspace (Supplementary Fig. 6). Conversely, antagonistic actuation, in which all six cables are pulled simultaneously, causes the entire trunk to contract from a relaxed length L_1 to a shorter, tensioned state L_2, resulting in a length variation $\Delta L = L_1 - L_2$. This contraction leads to a significant increase in stiffness, enabling the BRT to resist external forces and support payloads.

To quantify stiffness modulation, we conducted a quasi-static bending test using the setup in Fig. 3C. A mass M is suspended at the distal end of the BRT, and the resulting vertical deflection Δh is measured. The equivalent bending stiffness is calculated as $K = M\mathrm{g}/\Delta h$, providing a direct metric to evaluate stiffness under different levels of antagonistic contraction. The mechanical origins of this stiffness modulation are revealed in Fig. 3D, which depicts the deformation of connecting and reinforcing springs between two adjacent frames $\mathcal{F}_i$ and $\mathcal{F}_{i+1}$. The corresponding spring elongations are denoted as $\Delta l_{ci,m}$ (m = 1, …, 6) and $\Delta l_{\mathrm{r}i,n}$ (n = 1 and 2). Among them, reinforcing springs exhibit the largest elongation, increasing up to ~18 mm—approximately 4.5 times their pre-stretch length—as shown in Supplementary Fig. 7 and quantified in Table S2. The elastic energy stored in each spring is calculated as

$$W_{\mathrm{E\_c}i,m} = \int F_{ci,m}\mathrm{d}l_{ci,m} \text{ and } W_{\mathrm{E\_r}i,n} = \int F_{\mathrm{r}i,n}\mathrm{d}l_{\mathrm{r}i,n}.$$

where $F_{ci,m}$ and $F_{\mathrm{r}i,n}$ are the nonlinear force responses of the springs, respectively. The elastic energy stored in the connecting and reinforcing springs between frames $\mathcal{F}_i$ and $\mathcal{F}_{i+1}$ is $W_{\mathrm{E\_c}i} = \sum_{m=1}^{6} W_{E\_ci,m}$ and $W_{\mathrm{E\_r}i} = \sum_{n=1}^{2} W_{E\_ri,n}$, respectively. The total elastic energy accumulated in the structure is written as $W_{\mathrm{E}} = \Sigma\left(W_{\mathrm{E\_c}i} + W_{\mathrm{E}\_ri}\right)$, which approximately increases exponentially with ΔL as shown by both experimental and theoretical curves in Fig. 3E. Specifically, when ΔL= 0.3 m, the total energy increases by a factor of 7.23 compared to the uncontracted state. This energy buildup directly leads to increased stiffness. As shown in Fig. 3F, the bending stiffness K can be modulated from 23.94 N/m to 542.47 N/m, representing an order-of-magnitude range. These results align closely with model predictions from our nonlinear mechanical framework, detailed in Supplementary Notes (Supplementary Figs. 8-11)[54]. The model incorporates the nonlinear constitutive behavior of the springs (Supplementary Fig. 10) and accurately captures the relationship between contraction, deformation, and stiffness modulation (Supplementary Fig. 11), validating both the physical design and the analytical framework. This performance exceeds the typical range of conventional antagonistic systems, such as those using Ni-Ti alloys or silicone elastomers, which often suffer from low energy storage efficiency, poor deformation control, and instability issues like buckling[55]. In contrast, our BRT leverages distributed tension among many springs, ensuring rapid and scalable energy accumulation even with limited individual deformation. This design also improves durability and reusability, as the springs operate well below failure strain.

The functionality benefits of stiffness modulation are demonstrated in Fig. 3G. In a confined navigation task, the BRT bends around obstacles (Obstacle 1 and 2) while preserving overall morphology, as shown in the snapshots and Supplementary Fig. 12. At 20 seconds, the tip aligns above a balloon; with precise actuation, the needle-equipped distal end punctures the target at 24

seconds (Supplementary Movie 2), showing the robot's capability for fine motor execution under controlled stiffness. To further demonstrate load adaptability, we equipped the BRT with a 155.80 g robotic gripper and tested its ability to support objects of varying mass, from 0.07 to 2.17 kg. As shown in Fig. 3H, the BRT maintains a stable horizontal orientation while lifting diverse items including an egg, an apple, a tape roll, an electric drill, and a pack of coke. These results validate the robot's ability to dynamically adjust its stiffness for tasks ranging from fragile object manipulation to heavy payload support.

2.3 High-frequency stiffness modulation over a broader range

Beyond large-range tunability, the ability to modulate stiffness at high frequency is crucial for enabling robots to respond in real time to external stimuli, impact events, or task demands. The BRT achieves this capability through a high-speed actuation system composed of six independently driven cables, each controlled by a dedicated servo driver (Fig. 4A). This configuration allows rapid and coordinated cable contraction to dynamically alter the robot's structural stiffness within sub-second timescales. To experimentally validate this feature, we programmed the BRT to perform ten continuous stiffness switching cycles under three different modulation frequencies (Fig. 4B and Supplementary Fig. 13). The stiffness transitions, visualized as green, yellow, and orange trances, demonstrate that the robot can reliably and repeatedly cycle between soft and rigid states over a broad range—from 23.94 to 542.47 N/m—while maintaining structural integrity. This result highlights the robot's ability to adaptively tune its stiffness at a switching frequency of 1.06 Hz, comparable to that of biological systems such as elephant trunks.

The functional benefit of rapid stiffness modulation is demonstrated in an impact protection scenario. In the soft state, the BRT remains in a compliant state, and a 0.20 kg water bottle is dropped at 3.5 m/s onto an egg held by the distal gripper (Fig. 4C). Although the robot undergoes

passive deformation and absorbs part of the impact, the low stiffness is insufficient to prevent the egg from cracking, as shown in the inset in Fig. 4C. This highlights a critical limitation of soft robots: while compliant, they often lack the mechanical resilience to protect delicate payloads under impact. In contrast, when the BRT is pre-programmed to a high-stiffness state within 1 second, it exhibits enhanced impact resistance, absorbing the same collision without transferring damaging force to the egg (Fig. 4D). As a result, the egg remains intact without damage (Supplementary Movie 3). This rapid, reversible stiffness tuning capability allows the BRT to function not only as a compliant manipulator, but also as a protective structure capable of dynamically responding to unpredictable mechanical events. This capability is particularly relevant for applications in human-robot interaction and physical assistance, where both safety and responsiveness are essential.

Further, we evaluated the BRT's real-time adaptability to gradual loading conditions using a simulated infusion task. As shown in Fig. 4E and Supplementary Movie 4, a water bottle is incrementally filled from 0.06 kg to 0.65 kg over a 20-second period. The BRT continuously monitors the load and adjusts its cable tension in real time, increasing its internal contraction from ΔL=0.10 m to ΔL=0.24 m to maintain a stable horizontal posture. This experiment highlights the robot's ability to autonomously regulate its stiffness in response to slowly varying payloads without requiring manual intervention or recalibration. Moreover, the BRT can maintain an optimal balance between manipulation while achieving the necessary stiffness for stability and control[19]. For example, in Supplementary Fig. 14, the robot carries out manipulative tasks involving the transport of a filled bottle, adjusting its posture and stiffness accordingly. This capability is vital for tasks requiring simultaneous dexterity and strength, such as safe human interaction, mobile manipulation, and adaptable grasping.

2.4 BRT-assisted wheelchair with human-machine interface (HMI)

To demonstrate the practical utility and assistive potential of our BRT, we integrated it into an electric wheelchair equipped with a control module via human-machine interface (HMI)[56]. Embedding the variable-stiffness robotic arm into the wheelchair system substantially expands its functional capabilities beyond mobility support. The ability to tune stiffness not only improves task versatility, including delicate manipulations and stable load-bearing actions, but also ensures safer interactions in human-centered environments compared to the integration of rigid robotic arms (Table S3). Moreover, the wheelchair's mobility naturally complements the BRT's structural behavior: it compensates for the modest geometric shortening accompanying high-stiffness actuation, thereby preserving workspace and ensuring that the end-effector remains within reach of target objects.

As showcased in Fig. 5A and Supplementary Movie 5, the BRT is mounted to the side of the wheelchair and includes a cable-driven actuation and regulation unit, a soft robotic gripper, and an onboard camera attached to the end effector. The introduction of the robotic gripper has a decrease in the natural frequency of the BRT, as illustrated in Supplementary Fig. 15. This camera provides real-time visual feedback to the user via the HMI panel, allowing intuitive monitoring and alignment during manipulation tasks. The movement of the wheelchair is controlled by a joystick, enabling intuitive locomotion. Meanwhile, the HMI panel allows users to input commands for real-time stiffness modulation and access live video feed from a mounted camera (Fig. 5B). For ease of operation, users can also activate pre-programmed trajectories with a single click, such as folding and unfolding the robotic trunk or performing delivery actions. To accommodate non-programmed or flexible manipulation tasks, a secondary joystick is employed to manually guide the BRT. Upon joystick movement, the system first calculates length variations across the six

cables based on an inverse solution of mechanical models, then translates these into actuation commands for the servo systems (Supplementary Fig. 16). This control scheme enables both fine-grained customization and simplified user interaction, empowering users to perform complex manipulation tasks with minimal effort. The operational workflow is detailed in Fig. 5C. The user operates two joysticks simultaneously, one to control wheelchair motion and the other to manipulate the BRT. Once the gripper reaches the target object, the user can initiate a grasping action by simply rotating a rotary knob. This modular control logic separates locomotion from manipulation, offering a clear and accessible control scheme for users with diverse motor abilities.

To validate the precision and robustness of this control interface, we conducted a trajectory-tracking experiment in which the BRT was commanded to trace the English letters D, L, U, T using the joystick (Supplementary Movie 6). As shown in Fig. 5D, the robot successfully and accurately reproduces the letter contours, under both low-stiffness (ΔL=0.10 m, m = 0 kg) and high-stiffness (ΔL=0.20 m, m = 0.50 kg) conditions. These results demonstrate the stability, repeatability, and control precision of the BRT, even under varying mechanical configurations and payloads. Subsequently, vision-based control strategies are integrated. When an object enters the camera's field of view, the robotic arm can automatically align with the center of the object, thereby enhancing grasping accuracy (Supplementary Fig. 17, Supplementary Movie 7).

Moreover, to evaluate interaction safety, we measured contact forces during BRT sliding under different stiffness states using a thin-film sensor (Supplementary Fig. 18). Results show that even at high stiffness (366.63 N/m), the initial contact force remains low (5.45 N), and although peak force increasing during sliding due to geometric constraints, it remains within a controllable and safe range, showing that contact force can be effectively regulated via stiffness tuning. The combination of adaptive stiffness and user-friendly control ensures that individuals can manipulate

a variety of objects and perform diverse tasks with confidence and ease[57].

2.5 Validation of BRT-assisted wheelchair in real-world scenarios

To evaluate the practical utility of our BRT-assisted wheelchair in real environments, we conducted trails involving both a healthy individual and a post-stroke user, performing a variety of activities spanning indoor, outdoor, and social contexts. As shown in Supplementary Fig. 19, a healthy user is able to control the BRT-assisted wheelchair to complete tasks involving drug retrieval, safe delivery, and human-environment interaction. The robot's stiffness is adapted continuously to meet each task's physical requirements, confirming the system's versatility and operational reliability across realistic conditions.

As demonstrated in Fig. 6A, a post-stroke individual uses the system to complete essential activities of daily living in various real-world locations, such as retrieving meals in a restaurant, disposing of waste at a park, and grabbing drinks at a seaside. These trails show that the BRT can support individuals effectively in both public and private domains. In home environments, BRT with tunable stiffness allows users to perform diverse tasks with tailored compliance. For instance, in a soft state, the robot gently delivers lightweight objects like a remote control within reach, enabling the user to interact with household appliances (e.g., air conditioners), as shown in Fig. 6B and Supplementary Movie S8. For heavier tasks such as repositioning books, the user increases stiffness to ensure secure handling and accurate placement (Fig. 6C, Supplementary Movie 9).

Beyond tasks with a fixed stiffness requirement, many daily activities demand dynamic, multi-stage stiffness modulation. This includes placing objects in confined spaces or handling deformable items under load. As illustrated in Figs. 6D and 6E, the system adapts its stiffness in real time while placing a box in a cabinet or loading dirty clothes into a washing machine. The latter task (Fig. 6E, Supplementary Movie 10) involves a sequence of actions—opening the washer

door, repositioning a basket, transferring clothes, and closing the door—each requiring alternating between high stiffness for load-bearing and low stiffness for dexterous morphing. Using the joystick HMI and stiffness slider, the post-stroke individual successful completes this multi-step procedure within 371 seconds, demonstrating that the BRT's fast and broad-range stiffness modulation significantly reduces cognitive and physical burdens during self-care routines.

3. Discussion

Synergistic and antagonistic mechanisms have long served as a biologically inspired strategy for stiffness modulation in soft and continuum robots, yet existing designs often suffer from limited tunability and slow response[58]. Here, we developed a bionic robotic trunk (BRT) based on a cable-driven tensegrity skeleton, achieving dynamic stiffness modulation from 23.94 to 542.47 N/m with a switching frequency of 1.06 Hz, comparable to that of elephant trunks. One structural trade-off of our stiffness modulation strategy is the coupling between stiffness and manipulator length: antagonistic cable actuation shortens the trunk while increasing its stiffness. This trade-off is intrinsic to many tendon-driven designs, yet crucial—without structural shortening, the elastic energy that can be modulated remains limited, resulting in a narrow stiffness range. In our design, we utilize this shortening behavior to achieve high stiffness ratios, enabled by the geometric reconfiguration of the tensegrity skeleton. To address workspace concerns, we integrate the BRT into a mobile electric wheelchair platform. The wheelchair's mobility compensates for any length loss at high stiffness states, allowing the user to reposition the robot as needed and maintain full access to their environment.

While our system demonstrates promising results, it is important to acknowledge several limitations that must be addressed before widespread real-world deployment. First, both cable

creep and friction may affect long-term reliability and model accuracy. Future studies may address these issues by utilizing adaptive tensioning mechanisms and data-driven compensation methods. Second, the integration of additional sensors supports the advancement of robotic intelligence. For instance, incorporating force sensors in future configurations may prevent cable breakage by detecting overload conditions. Lastly, promoting active user engagement is essential for improving long-term outcomes. Future developments will focus on systematic evaluation across diverse user populations and real-world conditions. In addition, future systems will explore intent recognition, shared autonomy, and personalized control interfaces to increase accessibility.

4. Methods

4.1 Fabrication of a bionic robotic trunk

Three-dimensional (3D) computer-aided design models of frames were first built, and the number of frames in both middle and distal portions could be customized. Then, connecting and reinforcing springs were utilized to connect the frames, forming a tensegrity skeleton after putting on the tensioned cables with a diameter of 0.50 mm. In this BRT, the frames are 3D-printed using aluminum alloy, while the rest components are commercially available. To mitigate the effect of the morphing of the distal portion on the middle segment, the cables responsible for actuating the distal portion were connected to the actuation system by traversing through cable sheaths instead of the middle portion. Here, the sheaths are Teflon tubes with an outer diameter of 5.0 mm and an inner diameter of 2.0 mm. Then, black nylon fabric was applied to cover the surface of the skeleton. For the actuation system, six servo motors (ST10N40P10V2-AT1716, TECHSERVO, China) with reel installed were employed to selectively actuate the cables, enabling our BRT to deform.

4.2 Image-based measurement system

Our BRT was placed on a vibration isolator, and six marking points were evenly arranged at both the two ends of each portion. Then, a motion capture system (Prime 13, OptiTrack, USA) with 12 cameras was used to capture the movements of the marking points with a frame rate of 100 Hz. Utilizing experimental results obtained by this system, the robotic profile was reconstructed. The displacement of the points could be evaluated by comparing the position before and after morphing. According to the position of these points, the structural deformation was quantified, including length variation and bending angle.

4.3 Assembly of BRT-assisted electric wheelchair

The BRT-assisted electric wheelchair was composed of an electric wheelchair (DGN5001, YVEELT, China), a human-machine interface (HMI) panel (TD116, TouchWo, China), and our BRT equipped with a robotic gripper (M1520, YIZHUA ROBOT, China). The BRT was mounted on the right side of the wheelchair, while the HMI panel was positioned on the left side. To streamline user control, the joystick for operating the BRT and the rotary knob for controlling the gripper were integrated into a unified control box, symmetrically aligned with the wheelchair's original joystick to ensure intuitive operation. Additionally, both motor drivers (ADM-15D80-EALT, TECHSERVO, China) and a 24V lithium battery (24V50AH, AETLD BATTERY, China) were installed beneath the seat for optimal space utilization. The battery, with dimensions of 320 mm-240 mm-110 mm delivers continuous power for up to 10 hours, ensuring extended operational availability.

4.4 Human research participants

The recruited individual after brain stem bleeding is a 48-year-old Chinese male who consented to all the experiments and identifiable videos and images in this study with reasonable compensation. The authors affirm that human research participants provided informed consent for publication of the images in Figure 6. Rehabilitation exercises on the individual were conducted by protocols approved by Ethical Committee of Central Hospital of Dalian University of Technology (No. YN2024-133-20).

4.5 Statistical analysis

Experimental values were determined through a series of measurements conducted N times, followed by a statistical analysis carried out using specialized data analysis software. In cases where the experiment involved a single measurement ($N = 1$), only the raw data obtained from that measurement were reported. For experiments conducted multiple times ($N > 1$), the results were statistically processed, and the outcomes were presented in the figures as mean values accompanied by their corresponding standard deviations, i.e., means ± SD. This ensures a comprehensive representation of the data, providing insight into the central tendency of the experimental results.

Data availability

The authors declare that the main data supporting the findings of this study are available within the article and Supplementary Information files. All the relevant data is available at https://github.com/DUT-Jay/Data-Scource_BRT.git.

Reference

1 Schulz, A. K. *et al.* Elephant trunks use an adaptable prehensile grip. *Bioinspiration & Biomimetics* **18**, 026008 (2023).

2 Kaufmann, L. V., Becker, R., Ochs, A. & Brecht, M. Elephant banana peeling. *Current Biology* **33**,

R257-R258 (2023).

3 Dagenais, P., Hensman, S., Haechler, V. & Milinkovitch, M. C. Elephants evolved strategies reducing the biomechanical complexity of their trunk. *Current Biology* **31**, 4727-4737. e4724 (2021).

4 Wu, J. *et al.* Elephant trunks form joints to squeeze together small objects. *Journal of the Royal Society Interface* **15**, 20180377 (2018).

5 Peng, R., Wang, Y., Lu, M. & Lu, P. A dexterous and compliant aerial continuum manipulator for cluttered and constrained environments. *Nature Communications* **16**, 889 (2025).

6 Liu, W. *et al.* Touchless interactive teaching of soft robots through flexible bimodal sensory interfaces. *Nature Communications* **13**, 5030 (2022).

7 Leanza, S. *et al.* Elephant Trunk Inspired Multimodal Deformations and Movements of Soft Robotic Arms. *Advanced Functional Materials*, 2400396.

8 Zhang, J. *et al.* A preprogrammable continuum robot inspired by elephant trunk for dexterous manipulation. *Soft Robotics* **10**, 636-646 (2023).

9 Hu, Z., Zhang, Y., Jiang, H. & Lv, J.-a. Bioinspired helical-artificial fibrous muscle structured tubular soft actuators. *Science Advances* **9**, eadh3350 (2023).

10 Bishop, C., Russo, M., Dong, X. & Axinte, D. A novel underactuated continuum robot with shape memory alloy clutches. *IEEE/ASME Transactions on Mechatronics* **27**, 5339-5350 (2022).

11 Yang, C. *et al.* Geometric constraint-based modeling and analysis of a novel continuum robot with shape memory alloy initiated variable stiffness. *The International Journal of Robotics Research* **39**, 1620-1634 (2020).

12 Xing, Z., McCoul, D., Wang, F., Jin, T. & Zhao, J. Principle of stiffness variation based on matching composite structures with fibers. *Smart Materials and Structures* **29**, 095017 (2020).

13 Zhao, Y. *et al.* A soft continuum robot, with a large variable-stiffness range, based on jamming. *Bioinspiration & Biomimetics* **14**, 066007 (2019).

14 Yang, B. *et al.* Reprogrammable soft actuation and shape-shifting via tensile jamming. *Science Advances* **7**, eabh2073 (2021).

15 Robertson, M. A. & Paik, J. New soft robots really suck: Vacuum-powered systems empower diverse capabilities. *Science Robotics* **2**, eaan6357 (2017).

16 Zhang, J. *et al.* Bioinspired continuum robots with programmable stiffness by harnessing phase change materials. *Advanced Materials Technologies* **8**, 2201616 (2023).

17 Zhang, J. *et al.* Design and Stiffness Control of a Variable-Length Continuum Robot for Endoscopic Surgery. *IEEE Transactions on Automation Science and Engineering* (2024).

18 Zhang, Y. F. *et al.* Fast-response, stiffness-tunable soft actuator by hybrid multimaterial 3D printing. *Advanced Functional Materials* **29**, 1806698 (2019).

19 Chen, T. *et al.* Scale-inspired programmable robotic structures with concurrent shape morphing and stiffness variation. *Science Robotics* **9**, eadl0307 (2024).

20 Lin, B., Wang, J., Song, S., Li, B. & Meng, M. Q.-H. A modular lockable mechanism for tendon-driven robots: design, modeling and characterization. *IEEE Robotics and Automation Letters* **7**, 2023-2030 (2022).

21 Wang, T., Zhang, J., Li, Y., Hong, J. & Wang, M. Y. Electrostatic layer jamming variable stiffness for soft robotics. *IEEE/ASME Transactions on Mechatronics* **24**, 424-433 (2019).

22 Jadhav, S., Majit, M. R. A., Shih, B., Schulze, J. P. & Tolley, M. T. Variable stiffness devices using fiber jamming for application in soft robotics and wearable haptics. *Soft Robotics* **9**, 173-186 (2022).

23 Wang, Y., Li, L., Hofmann, D., Andrade, J. E. & Daraio, C. Structured fabrics with tunable mechanical properties. *Nature* **596**, 238-243 (2021).

24 Hao, Y., Gao, J., Lv, Y. & Liu, J. Low melting point alloys enabled stiffness tunable advanced materials. *Advanced Functional Materials* **32**, 2201942 (2022).

25 Mao, L. *et al.* Magnetic steering continuum robot for transluminal procedures with programmable shape and functionalities. *Nature Communications* **15**, 3759 (2024).

26 Yang, Y., Li, Y. & Chen, Y. Principles and methods for stiffness modulation in soft robot design and development. *Bio-Design and Manufacturing* **1**, 14-25 (2018).

27 Fan, Y., Yi, B. & Liu, D. An overview of stiffening approaches for continuum robots. *Robotics and Computer-Integrated Manufacturing* **90**, 102811 (2024).

28 Xing, Z. *et al.* A structure for fast stiffness-variation and omnidirectional-steering continuum manipulator. *IEEE Robotics and Automation Letters* **6**, 755-762 (2020).

29 Schulz, A. K. *et al.* Skin wrinkles and folds enable asymmetric stretch in the elephant trunk. *Proceedings of the National Academy of Sciences* **119**, e2122563119 (2022).

30 Dou, W. *et al.* Soft robotic manipulators: Designs, actuation, stiffness tuning, and sensing. *Advanced Materials Technologies* **6**, 2100018 (2021).

31 Kim, Y., Cheng, S. S. & Desai, J. P. Active stiffness tuning of a spring-based continuum robot for MRI-guided neurosurgery. *IEEE Transactions on Robotics* **34**, 18-28 (2017).

32 Althoefer, K. Antagonistic actuation and stiffness control in soft inflatable robots. *Nature Reviews Materials* **3**, 76-77 (2018).

33 Yi, B., Fan, Y., Liu, D. & Romero, J. G. Simultaneous position-and-stiffness control of underactuated antagonistic tendon-driven continuum robots. *IEEE Transactions on Automation Science and Engineering* (2024).

34 Wang, P., Zang, J., Dong, Z., Xing, Z. & Zhao, J. Design and Statics Model of an Extensible Hybrid-Driven Continuum Robot with Variable Stiffness. *Sensors and Actuators A: Physical*, 116177 (2025).

35 Ikemoto, S., Tsukamoto, K. & Yoshimitsu, Y. Development of a modular tensegrity robot arm capable of continuous bending. *Frontiers in Robotics and AI* **8**, 774253 (2021).

36 Chen, D. *et al.* Design and analysis of a novel bionic tensegrity robotic fish with a continuum body. *Biomimetics* **9** (2024).

37 Harsono, E., Yang, J., Bhattacharya, S. & Yu, H. Design and analysis of a novel hybrid-driven continuum robot with variable stiffness. *Mechanism and Machine Theory* **177**, 105067 (2022).

38 Kim, Y.-J., Cheng, S., Kim, S. & Iagnemma, K. A stiffness-adjustable hyperredundant manipulator using a variable neutral-line mechanism for minimally invasive surgery. *IEEE Transactions on Robotics* **30**, 382-395 (2013).

39 Wang, P., Guo, S., Wang, X. & Wu, Y. Design and analysis of a novel variable stiffness continuum robot with built-in winding-styled ropes. *IEEE Robotics and Automation Letters* **7**, 6375-6382 (2022).

40 Huang, D., Yang, L. & Sun, Y. in *International Conference on Intelligent Robotics and Applications.* 429-441 (Springer).

41 Shah, D. S. *et al.* Tensegrity robotics. *Soft Robotics* **9**, 639-656 (2022).

42 Zhang, J. *et al.* Bio-inspired tensegrity building block with anisotropic stiffness for soft robots. *IEEE/ASME Transactions on Mechatronics* (2025).

43 Jeon, H. *et al.* Towards a snake-like flexible robot with variable stiffness using an SMA spring-based friction change mechanism. *IEEE Robotics and Automation Letters* **7**, 6582-6589 (2022).

44 Clark, A. B. & Rojas, N. Assessing the performance of variable stiffness continuum structures of large diameter. *IEEE Robotics and Automation Letters* **4**, 2455-2462 (2019).

45 Kang, J., Lee, S. & Park, Y.-L. Soft bending actuator with fiber-jamming variable stiffness and fiber-optic proprioception. *IEEE Robotics and Automation Letters* (2023).

46 Hu, J., Xiao, C. & Wen, T. A novel tunable stiffness mechanism using filament jamming. *Journal of Mechanisms and Robotics* **13**, 061015 (2021).

47 Al Abeach, L., Nefti-Meziani, S., Theodoridis, T. & Davis, S. A variable stiffness soft gripper using granular jamming and biologically inspired pneumatic muscles. *Journal of Bionic Engineering* **15**, 236-246 (2018).

48 Fang, B. *et al.* Multimode grasping soft gripper achieved by layer jamming structure and tendon-driven mechanism. *Soft Robotics* **9**, 233-249 (2022).

49 Yang, C. *et al.* A flexible gripper with a wide-range variable stiffness structure based on shape memory alloy. *Industrial Robot: the International Journal of Robotics Research and Application* **49**, 1190-1201 (2022).

50 Liao T, Kalairaj M S, Cai C J, et al. Fully-printable soft actuator with variable stiffness by phase transition and hydraulic regulations[C]//*Actuators*. MDPI, 2021, 10(10): 269.

51 Hu, C. *et al.* A miniaturized variable stiffness soft manipulator with a customizable LMPA pattern. *IEEE Robotics and Automation Letters* (2023).

52 Zhang, Z. *et al.* Design and analysis of hybrid-driven origami continuum robots with extensible and stiffness-tunable sections. *Mechanism and Machine Theory* **169**, 104607 (2022).

53 Park, M. *et al.* Deployable soft origami modular robotic arm with variable stiffness using facet buckling. *IEEE Robotics and Automation Letters* **8**, 864-871 (2022).

54 Li, F., Yang, H., Gu, G., Wang, Y. & Peng, H. Position and Orientation Tracking Control of a Cable-Driven Tensegrity Continuum Robot. *IEEE Transactions on Robotics* (2025).

55 Peyron, Q. & Burgner-Kahrs, J. Stability analysis of tendon driven continuum robots and application to active softening. *IEEE Transactions on Robotics* (2023).

56 Sui, M. *et al.* A soft-packaged and portable rehabilitation glove capable of closed-loop fine motor skills. *Nature Machine Intelligence* **5**, 1149-1160 (2023).

57 Liang, X. *et al.* Design, characterization, and implementation of a two-DOF fabric-based soft robotic arm. *IEEE Robotics and Automation Letters* **3**, 2702-2709 (2018).

58 Lin, B., Song, S. & Wang, J. Variable stiffness methods of flexible robots for minimally invasive surgery: A review. *Biomimetic Intelligence and Robotics*, 100168 (2024).

Acknowledgements

This work is supported by Natural Science Foundation of Liaoning Province Program (No.

2024JH3/50100003 and No. 2025080026-JH3/101), China Postdoctoral Science Foundation (2025M781273), and Postdoctoral Fellowship Program of CPSF (No. GZC20240192).

Author contributions statement

Conceptualization: J.Z., X.J., and H.P. Methodology: J.Z., C.Y., H.Y., T.Z., and H.P. Investigation: J.Z., C.Y., P.M., C.H, and X.W. Visualization: J.Z., C.Y., K.L., X.J, and H.P. Funding acquisition: J.Z. and H.P. Supervision: X.J., and H.P. Writing-original draft: J.Z., C.Y., and X.J. Writing-review and editing: J.Z., X.J., and H.P.

Competing interest statement

The authors declare no competing interests

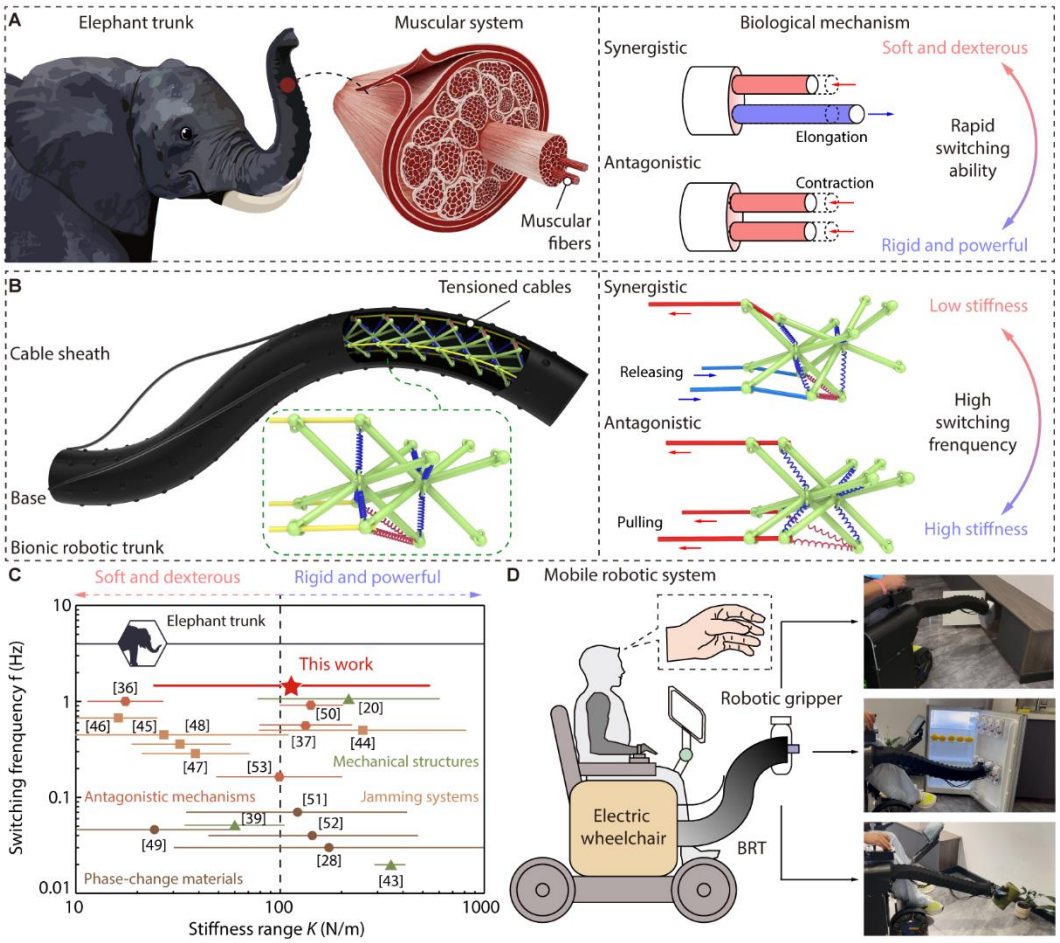

Fig. 1. A tensegrity-based bionic robotic trunk (BRT) with the stiffness modulation mechanism inspired by an elephant trunk. (A) The elephant trunk consists of a complex muscular system that enables synergistic and antagonistic muscle actions for stiffness modulation Synergistic activation contracts/elongates opposing muscles, allowing for soft and dexterous movements, whereas antagonistic contraction generates internal tension, increasing rigidity and load-bearing capacity. (B) The BRT is constructed with a cable-driven tensegrity skeleton, where tensioned cables mimic the muscular structure. Synergistic activation releases cable tension for low stiffness, while antagonistic contraction increases elastic potential energy, achieving high stiffness at a fast-switching frequency. (C) Comparison of the stiffness variability and switching frequency between BRT and existing robotic trunks[20,28,36,37,39,43-53]. (D) Integration of the BRT into a mobile robotic system for assistive applications, including opening cabinet doors, retrieving items form a refrigerator, and watering flowers.

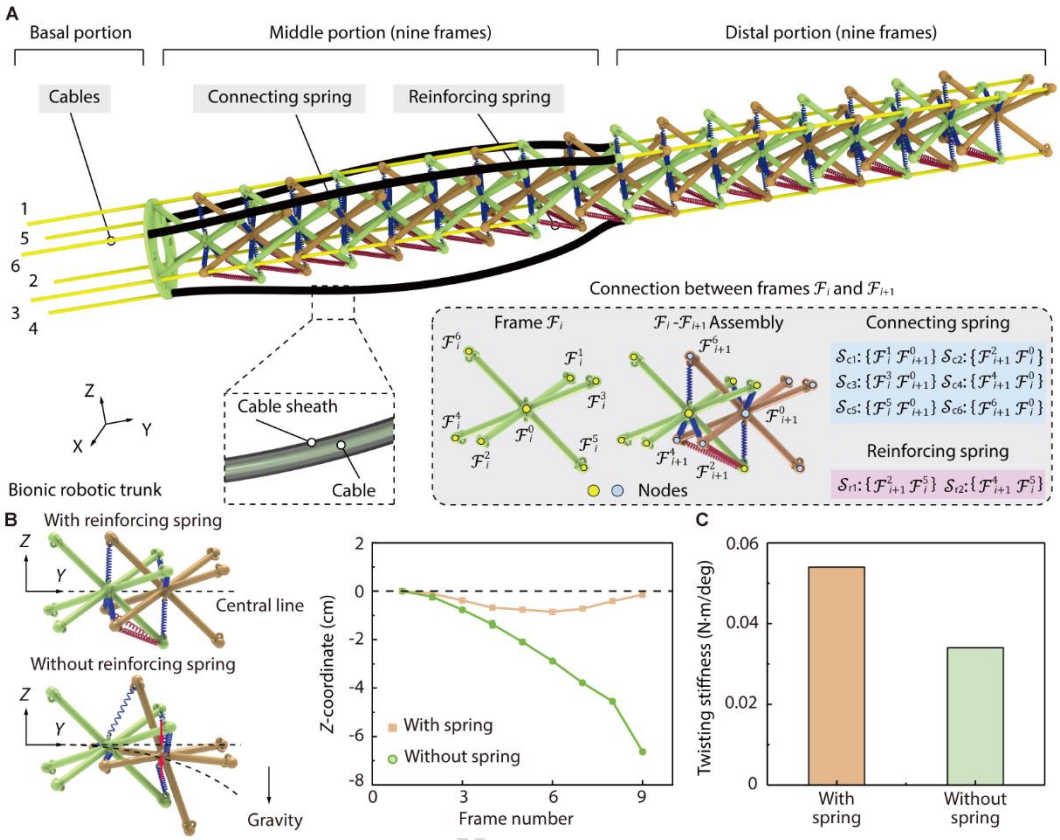

Fig. 2. Tensegrity-based design of the BRT. (A) The trunk consists of basal, middle, and distal portions, each composed of multiple tensegrity frames $\mathcal{F}_i$ connected via cables, connecting springs, and reinforcing springs. The cable sheath encases the internal cables to avoid physical interference between cables. A detailed schematic illustrates the connection between adjacent frames, where connecting springs (blue) and reinforcing springs (purple) enhance structural integrity. (B) Comparison between the BRT with and without reinforcing springs shows that the reinforced structure maintains a more centralized alignment, while the non-reinforced version exhibits greater deformation due to gravity. The Z-coordinate of the centerline plot quantifies the structural sagging, demonstrating improved stability with reinforcing springs. (C) The reinforcing springs enhance twisting stiffness for improved structural integrity.

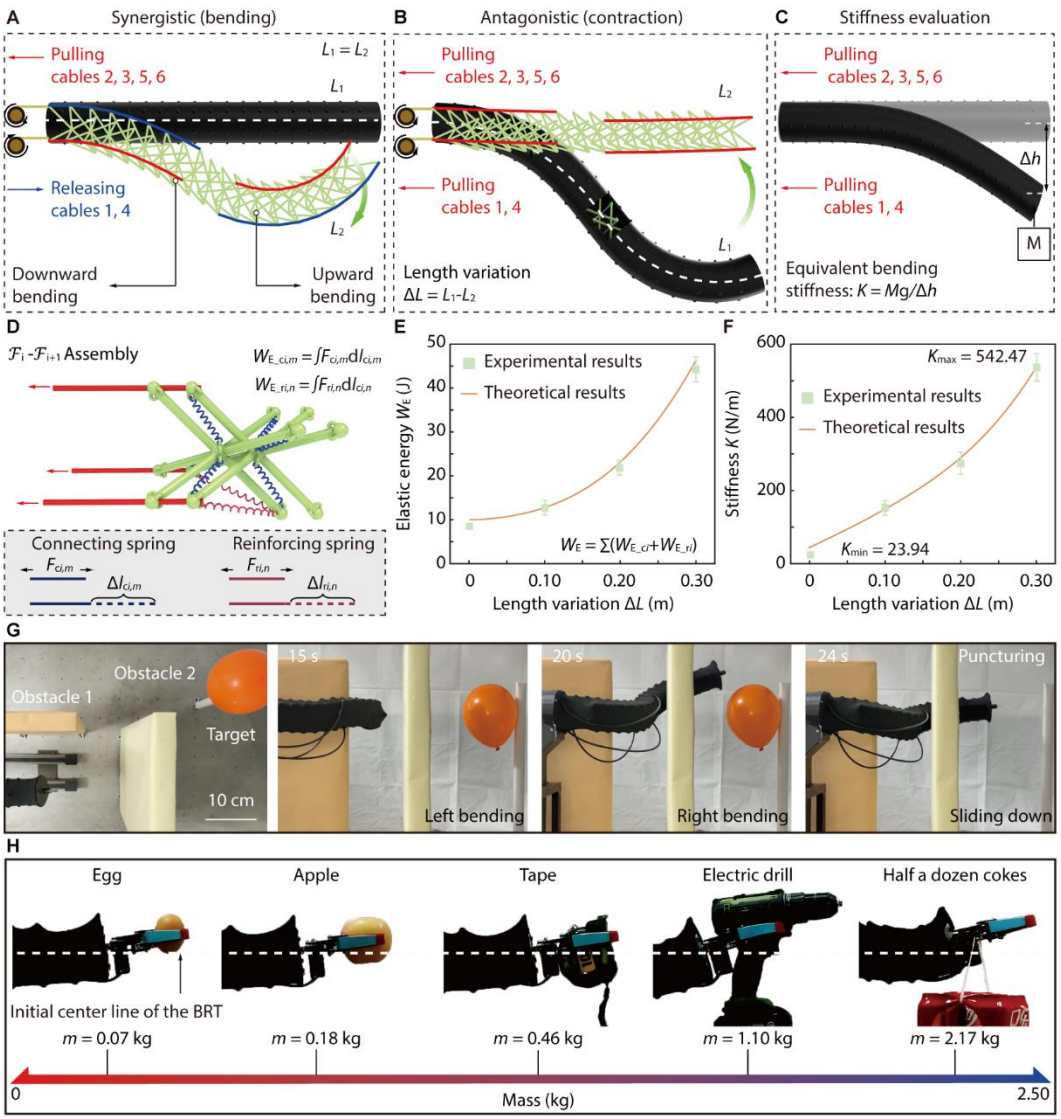

Fig. 3. Tensegrity-enabled large-scale stiffness modulation. (A) In the synergistic mode, opposing cable actions (e.g., pulling cables 2, 3, 5, 6 and releasing cables 1, 4) induce S-shaped bending, enabling a low-stiffness configuration with structural length L_1. (B) In the antagonistic mode, all cables are pulled to generate internal contraction, shortening the structure to length L_2 and increasing stiffness. The length variation is defined as $\Delta L = L_1 - L_2$. (C) Stiffness evaluation method, where a vertical displacement Δh of the distal end is caused by a suspended mass M, yielding equivalent bending stiffness $K = Mg/\Delta h$. (D) Internal mechanics of a frame-to-frame assembly, showing deformation of connecting and reinforcing springs during contraction. Their respective elastic energies are denoted as $W_{E\_ci,m}$ and $W_{E\_ri,n}$. (E) Measured and simulated total elastic energy W_E as a function of ΔL. (F) Bending stiffness K versus length variation ΔL, showing a large tunability from 23.94 to 542.47 N/m. (G) Demonstration of the BRT navigating through confined obstacles and puncturing a target, enabled by real-time stiffness adaptation. (H) The two-segment BRT adapts its stiffness to stably support objects of varying mass (0-2.50 kg) while

maintaining a constant horizontal orientation, illustrating robust load-bearing control through stiffness modulation.

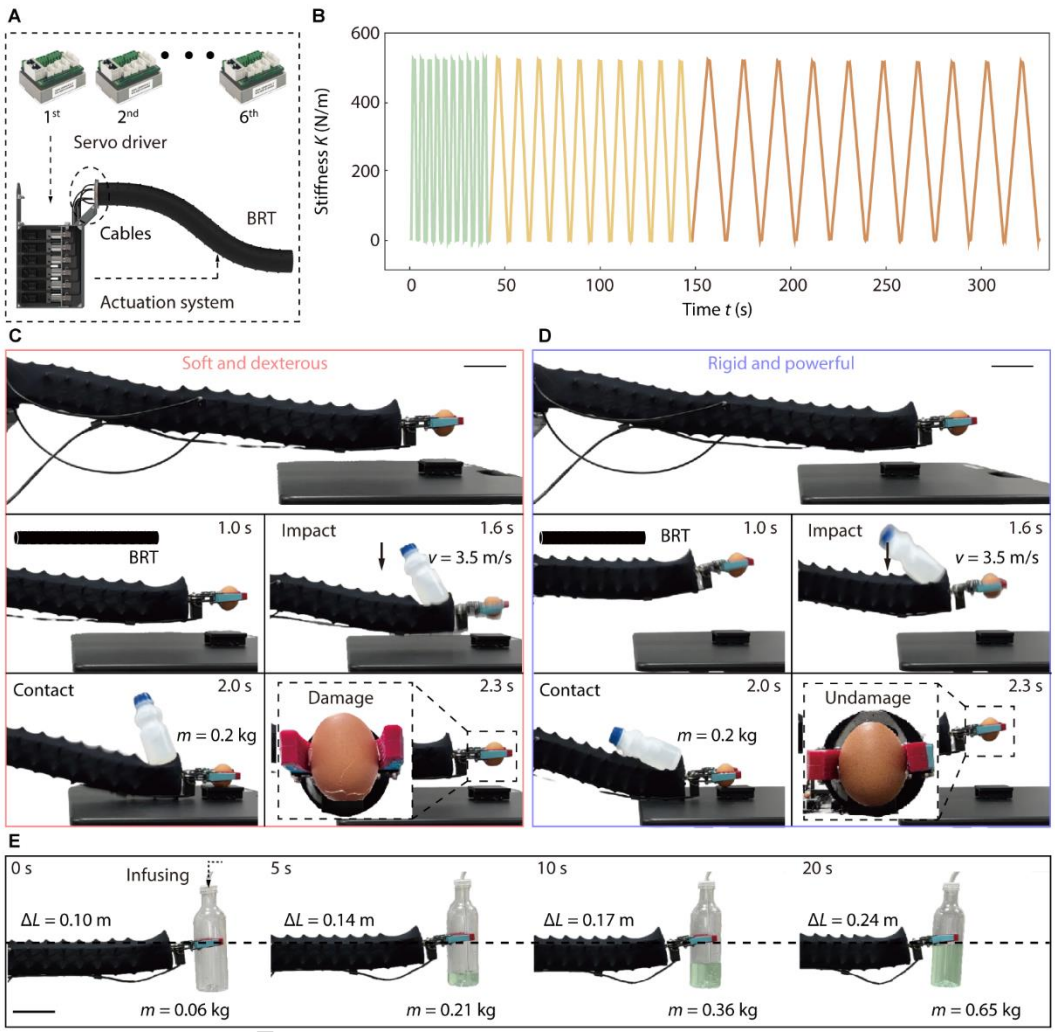

Fig. 4. High-frequency stiffness modulation over a broader range. (A) Experimental setup of the BRT with six independently actuated cables driven by servo motors. (B) Real-time demonstration of dynamic stiffness modulation across three frequencies, marked by green, yellow, and orange lines. For each case, BRT undergoes ten stiffness switching cycles, showcasing rapid and repeatable transitions. (C) In the soft state, the BRT remains compliant under external impact (v = 3.50 m/s, m = 0.20 kg), but the gripped egg is damaged due to insufficient impact mitigation. (D) When the robot is programmed to a rigid state within 1 second, its increased stiffness absorbs the impact and prevents egg breakage, demonstrating protective behavior through rapid stiffness adjustment. Scale bar: 10 cm. (E) During a simulated infusion process, the BRT dynamically tunes its stiffness in response to a gradually increasing payload from 0.06 to 0.65 kg. The structure remains stable across a corresponding contraction (ΔL) range from 0.10 m to 0.24 m, effectively supporting the varying load without sagging.

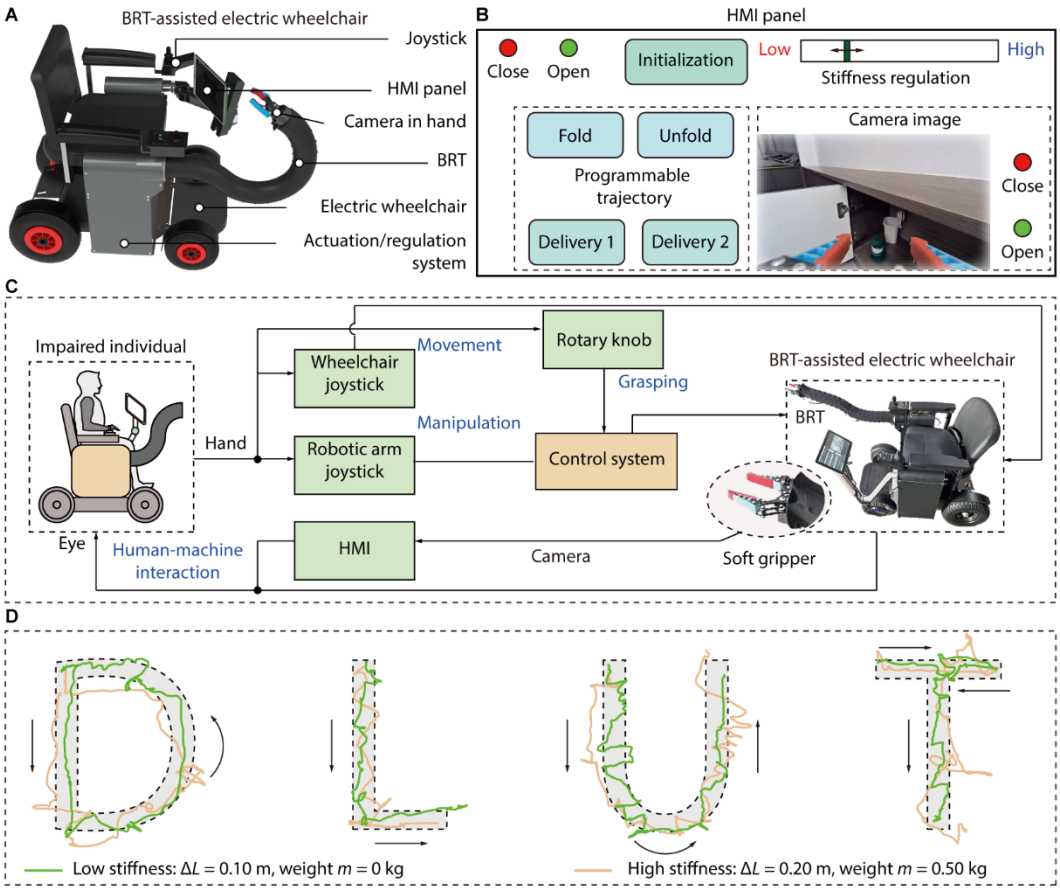

Fig. 5. BRT-assisted electric wheelchair with human-machine interface (HMI). (A) Schematic illustration of the BRT-assisted electric wheelchair system, which integrates an electric wheelchair, BRT, and HMI panel. A camera is mounted on the robotic gripper to provide real-time visual feedback. (B) HMI panel for user interaction, enabling control of stiffness regulation, gripper operation, and predefined manipulation functions. (C) Operational workflow of the assistive system. During manipulation, users operate two joysticks to control the wheelchair and the robotic trunk independently. Once the gripper is aligned with the target, the task is executed via a rotary knob. (D) Demonstration of joystick-based control for trajectory tracking, where the BRT traces the English letters D, L, U, and T.

Fig. 6. Validation of the BRT-assisted wheelchair in real-world scenarios by a post-stroke individual. (A) The BRT-assisted electric wheelchair supports daily activities across diverse real-life environments, including a restaurant, supermarket, park, and seaside. (B) Task: Pick up the remote control. The BRT operates in a low-stiffness mode to enable compliant reaching and gentle grasping of lightweight objects. (C) Task: Put the book on the shelf. The robot maintains a high-stiffness state to support the weight of the book and ensure precise placement on an elevated shelf. (D) Task: Put the box in the cabinet. The BRT dynamically modulates between high and low stiffness to navigate confined space and execute stable placement. (E) Task: Put dirty clothes into the washing machine. The system adjusts stiffness in real time to facilitate both flexible positioning and robust object transfer, adapting to changes in posture and load.

Editorial Summary

Authors present a bionic robotic trunk with a cable-driven tensegrity skeleton, leveraging synergistic and antagonistic muscle-mimicking mechanisms to achieve rapid and large-range stiffness modulation comparable to that of an elephant trunk.

Peer review information: *Nature Communications* thanks the anonymous reviewer(s) for their contribution to the peer review of this work. A peer review file is available.